Engineering Science and Military Technologies
Volume (6) - Issue (2) - Sep 2022
ISSN: 2357- 0954
DOI:10.21608/EJMTC.2022.166266.1238

Original Article

Design and implementation of embedded servo control system for a high maneuvering Ariel vehicle

Mohammed Etewa, Gamal A. Elnashar, Ahmed Mohsen Kamel, Hossam Hendy

Military Technical College, Cairo, Egypt

Keywords:
Driving circuit, embedded system, inrush current, position control, pneumatic system.

Corresponding Author: Mohammed Etewa, Military Technical College, Cairo, Egypt, **Tel**: +201006381777, **Email**: mohammed.etewa86@gmail.com

Abstract
This research demonstrates the procedure for servo control circuit implementation for the guided missile. Motivated by enhancing the performance of the guided missile servo system control circuit by using embedded systems and gaining the digital circuit advantages and, solving the problem of obsolete analog components. The proposed servo system includes four servo pistons for driving the missile canard. A high-resolution gear potentiometer is used as positionfeedback for the missile fin. The guidance command converted from the polar form to cartesian and delivered as input to the microcontroller PIC18f4431 to control the pneumatic servo by generating corresponding pulse width modulation(PWM) to the driving circuit.In this regard System identification for the pneumatic servo system is carried out. In current work,a servo positioning system based on an embedded system was designed to achieve a deterministic time response and minimize the jitters around 155µs for accurate guidance and control operation. The accuracy of the controlled system was verified using servoAutomatic Test Equipment (ATE) and,the results show the enhancement in the platform performance based on digital implementation instead of the analog circuit.

1. INTRODUCTION

The pneumatic servo system with its numerous advantages makes it very attractive to researchers including a high power-to-weight ratio, low cost, long lifetime, and cleanliness[1].

However, it introduces nonlinear characteristics that make the pneumatic servo more uncertain such as the pressure in the cylinder, nonlinear frictional forces, and time-varying load that entailed a sophisticated closed-loop control design to control the servo proportional valve[2]. The revolution in applied mathematics and computational capabilities simplifies the design and implementation of the flight control system controller. In addition, the developments in microprocessors and embedded systems and their availability with less cost, size, and weight attract many researchers all over the world towards embedded systems especially flight control based on an embedded system.

In current work,typical servo control circuits are still in service based on analog control circuits that drive the missile servo system[3]. As a consequence, many components of missile servo control systems are outdated, andbecame harder to replace the malfunctioning parts. With the great developments in embedded systems and CAD simulation tools, the design and implementation of missile servo control circuits are facilitated. The work presented in this research is concerned with improving the performance of pneumatic servo system control circuits based on an embedded system.

In addition, QAD (Quadrature Amplitude Demodulation) is applied for the coordinate transformation of the guidance command signal in order to control the servo system[4].

The missile servo system control circuit has been implemented based on a microcontroller embedded system which is programmed under the MikroCTM environment to generate the required PWM that controls the four pneumatic solenoids in the driving circuit. System identification for the pneumatic servo system is carried out to facilitate the design of the proper controller of the missile pneumatic servo system[2].

The final prototype of the servo system control circuit is tested and evaluated using ATE (Automatic Test Equipment) servo performance test stations.

The structure of this research is as follows; section 2 presents the pneumatic servo section structure. Section 3 presents system identification for the pneumatic servo section. Section 4 presents QAD circuit. Section 5 presents the servo controller design. Section 6 presents the driving circuit solution.The ATE results compared with the original . performance are highlighted in section 6. Finally, the study isconcluded in section 7

Nomenclature	
u_1	Input Voltage
y_1	Output fin deflection
BJ	Box-Jenkins Model
OE	Output-Error Model
SS	State-Space
TF	Transfer Function
$\varphi(t)$	Periodic half-wave symmetric function
Z	Impedance
R	Resistance
L	Inductance

2-Proposed Servo Section Structure

The servo section, shown in Figure (1), consists of the rocker arms, solenoid pistons, relief valve,and feedback gear resistor. The function of the servo section is to execute the missile steering by applying torques to the fins.The differential piston pressure rotates a rocker arm to which a pair of fins is mounted. Rotation of the rocker's arm deflects the fins in the air stream until the torque on the fins from the airstream is just equal to the torque delivered by the servo. Additionally, the gear potentiometers on the rocker's arms provide fin current position feedback for accurate control at low torque command. Those pistons driven through the output signals from the amplifiers control two sets of push-pull solenoids Pistons act in pairs, up/down and right/left. As the current is increased in one piston solenoid valve, the current in the opposite piston solenoid valve is reduced so the amount of gas is released and the steering executed[2].

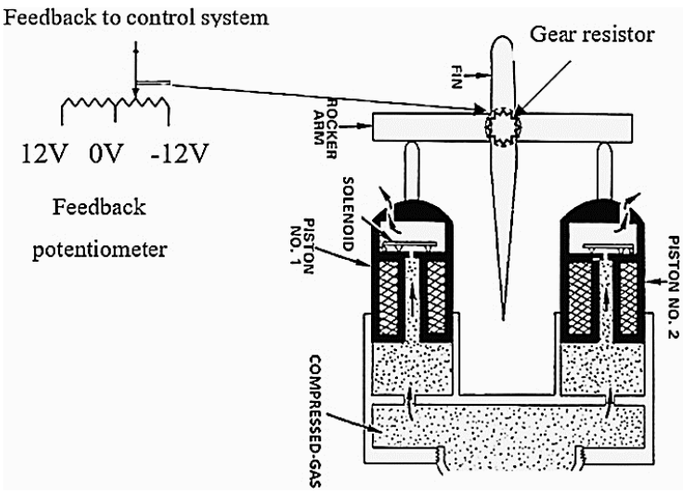

Fig. 1: Schematic of pneumatic servo section

3- Pneumatic Servo System Identification and Analysis

The system model should predict the input-output response in such a way that can be used to design a controller with a high confidence level to work with the real physical system[5]. There are two ways to get a system model the first one is to apply the laws of physics to a certain phenomenon with known physical parameters while the second one is by conducting experiments on the physical system itself with systems identification. The second approach utilizes the processor in the loop simulation.Based on parametric method necessitates, a specific controller model structure in which the parameters are estimated using the observed input/output data[6]. The servo section is disassembled from a real missile and interfaced with the microcontroller and applies a simulation program for the input on the microcontroller then measures the servo system output by the microcontroller analog to digital converters.The output signals from the driving circuits control two sets of push-pull solenoids. As the current is increased in one piston solenoid valve by increasing PWM duty cycle, the current in the opposite piston solenoid valve is reduced by reducing PWM duty cycle. The resulting differential piston pressure rotates a rocker arm to which a pair of fins is mounted. The potentiometers on the rocker's arms provide fin position feedback for accurate fine control. The pneumatic servo system transfer function is estimated using an experiment. In this experiment, the actuator driver output voltage is the input $u_1$while the fin deflection is the output y_1 measured withthe potentiometer value measured by the microcontroller ADC (Analog-to-Digital Converter).The transfer function parameters of the pneumatic servo are identified according to the input/output data as shown in Figure (2).

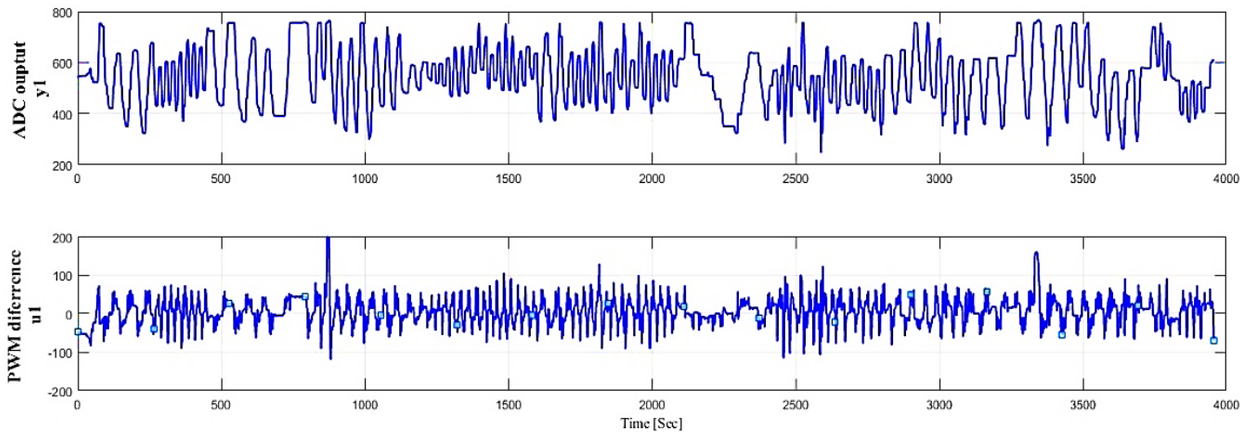

Fig. 2: Servo Row input/output signal for Sys.idetification

The identification process amounts to repeatedly picking a model, computing the best model in the structure, and evaluating this model's performance to justify its satisfaction[7]. This cycle can be itemized as follows:

Step1: Design an experiment and collect input-output data from the process or system to be identified.

Step2: Examine the data, polish it to remove trends and outliers, and select useful portions of the original data.

Step3: Estimating input delay to gain a better insight into the dynamics via obtaining the impulse response of the system.

Step4: Select and define a model structure (a set of candidate system descriptions) within which a model is to be found.

Step5: Compute the best model in the selected model structure according to the input-output data and the given fit criterion.

Step6: Examine the obtained model's properties (residuals - noise spectra - pole-zero configurations).

Step7: If the model is good enough, then stop; otherwise go back to the fourth step to try another model set. Possibly also try another estimation method in the fifth step or work further on the input-output data in the first and second steps.

The Identification Toolbox in MATLAB[8] proposes several functions for every step. For the second step, there are procedures to remove trends in data, plot data, and filter data as well as to resample and recreate missing data. For the third step, the impulse function was used to analyze a non-parametric impulse response. This response is drawn with a conviction interval signified by 3 standard deviations. The fourth step recommends a variety of nonparametric models, as well as all the most common black-box input-output and state-space structures in addition to linear state-space models in discrete and continuous time, are made by a general tailor. For the fifth step general prediction error (maximum likelihood) methods, as well as sub-space methods and instrumental variable methods are offered for parametric models, while spectral analysis methods and basic correlation are used for nonparametric model structures. To investigate models in the sixth step, many functions allow the calculation and presentation of frequency functions with poles and zeros, as well as simulation and prediction using the model. Functions are also included for transformations between discrete-time and continuous-time model descriptions. Therefore, a MATLAB environment is created (conducts the system identification steps) to identify transfer function models for the implemented hardware using experimental data from the flight simulation model. The identified transfer function of the servo actuator in discrete form and converted to third order continuous form using different model structures including ARX, ARMAX, BJ, OE transfer function, and state space model as shown in Figure (3) and BJ is the best fitting model[9]. Discrete-time BJ model is:

$$y(t) = [B(z)/F(z)]u(t) + [C(z)/D(z)]e(t) \quad (1)$$

$$B(z) = 0.4419z^{-1} - 0.4397z^{-2} \quad ,C(z) = 1 - 0.4208z^{-1} - 0.5581z^{-2} \quad (2)$$

$$D(z) = 1 - 1.959z^{-1} + 0.9718z^{-2}, F(z) = 1 - 1.969z^{-1} + 0.969z^{-2} \quad (3)$$

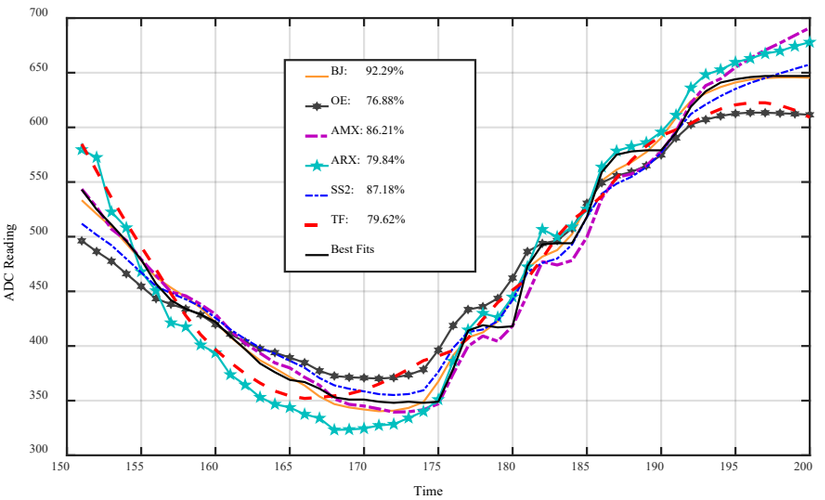

Fig. 3: Validation of different estimation models

4-Implementation of Quadrature Amplitude Demodulation Circuit:

The guidance command signalwhen an error is presentis the summation of 2 modulated signals sine which is U/D signal and cosine which is R/L signal synchronized with R/L and U/D reference signal. According to the reference signal, the direction of the fin deflection is determined. The amplitude for the sine determines how much deflection it will be and the sign determines the direction UP or DOWN. The same sequence is applied for the cosine signal which represents the R/L plane.

In the demodulation circuit, as showninFigure (4) the guidance command signal is multiplied by the U/D reference signal to extract the U/D error signal as DC voltage positive or negative according to the sign of the sine component in the guidance command signal and the value related to the sine amplitude value.

In the proposed design the guidance command signal is multiplied by the R/L reference signal to extract the R/L error signal as D.C voltage positive or negative according to the sign of the cosine component in the guidance command signal and the value related to the cosine amplitude value.

Quarter-wave symmetric functions: If a periodic function φ(t) has half-wave symmetry and, in addition, is either an even or odd function, As represented in Figure (5) up/down reference signal is aperiodic odd quarter-wave symmetric with amplitude value (a)[10],The odd quarter wave symmetry function Y_1 (t) shown Figure (5) is given as follows:

$$Y_1(t) = -Y_1(t \pm T/2)$$
$$Y_1(t) = -Y_1(-t) \qquad (4)$$

Where the Fourier series will :

$$Y_1(t) = \sum_{n=1}^{\infty} a[2n-1](\sin((2n-1)\omega t)) \qquad (5)$$

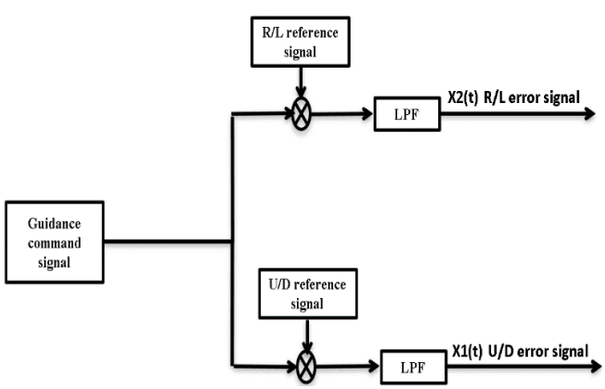

Fig. 4: Guidance command signal demodulation

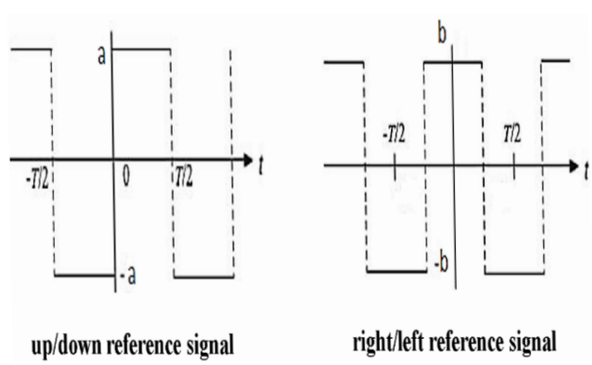

Fig. 5: Reference signals

By similarity, the R/L reference signal in Figure (5) is an even quarter-wave symmetric

$$Y_2(t) = -Y_2(t + T/2) \qquad (6)$$

Consequently, the right/left reference signal is even quarter-wave symmetric, Where the Fourierseries will be :

$$Y_2(t) = \sum_{n=1}^{\infty} a[2n-1](\cos((2n-1)\omega t)) \qquad (7)$$

The input guidance command signal is:

$$m_1 \cos(\omega t) + m_2 \sin(\omega t) \qquad (8)$$

$$X_1(t) = [m_1 \cos(\omega t) + m_2 \sin(\omega t)][\sum_{n=1}^{\infty} a[2n-1](\cos((2n-1)\omega t))]$$

$$= [m_1 \cos(\omega t) + m_2 \sin(\omega t)][a\cos(\omega t) + 3a\sin(3\omega t) + ...]$$

$$= \left[a \times m_1 \cos^2(\omega t)\right] + \left[a \times m_2 \sin(\omega t)\cos(\omega t)\right] + \left[3a \times m_1 \cos(\omega t)\cos(3\omega t)\right] + \left[3a \times m_2 \sin(\omega t)\cos(3\omega t)\right] + \cdots$$

$$= \left[.5a \times m_1 + \left(.5a \times m_1 \cos(2\omega t)\right)\right] + \left[.5a \times m_2 \sin(2\omega t)\right] + \left[1.5a \times m_1 \left(\cos(4\omega t) + \cos(2\omega t)\right)\right] + \left[1.5a \times m_2 \left(\sin(4\omega t) + \cos(2\omega t)\right)\right] + \cdots$$

Will be cancelled with the low pass filter

$$X_1(t) = 0.5a \times m_1 \qquad (9)$$

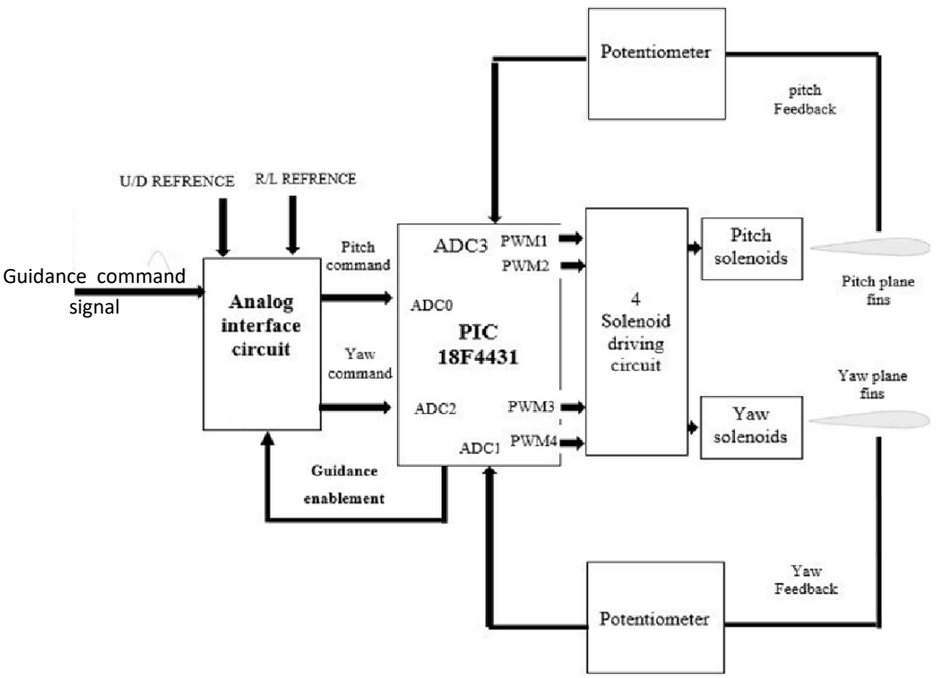

Fig. 6: Structure Diagram ofthe Missile Control System

From eq.(9) the up/down plane error signal after filtering will be DC voltage, similarly, the multiplier output x_2 (t) in Figure (4) the guidance command error signal for the right/left plane will be as follows:

$$X_2(t) = 0.5b \times m_2 \qquad (10)$$

From eq.(10) the up/down plane error signal after filtering becomes DC voltage. Where the polarity for this DC determines which direction fins will deflect and the amplitude determine how much there will be.

As shown in Figure 7 and Figure 8 the input signals for this stage are simulated. Where, if the input command signal coincidence with the up-down reference signal it means that "It's a pure Down command" and if it is a coincidence with the negative sign it's pure Up. To make deflection in both planes, the input command signal while having a componentin two planes that is not pure sine or cosine. Figure 7 and Figure 8 the simulation for a demodulation stage.

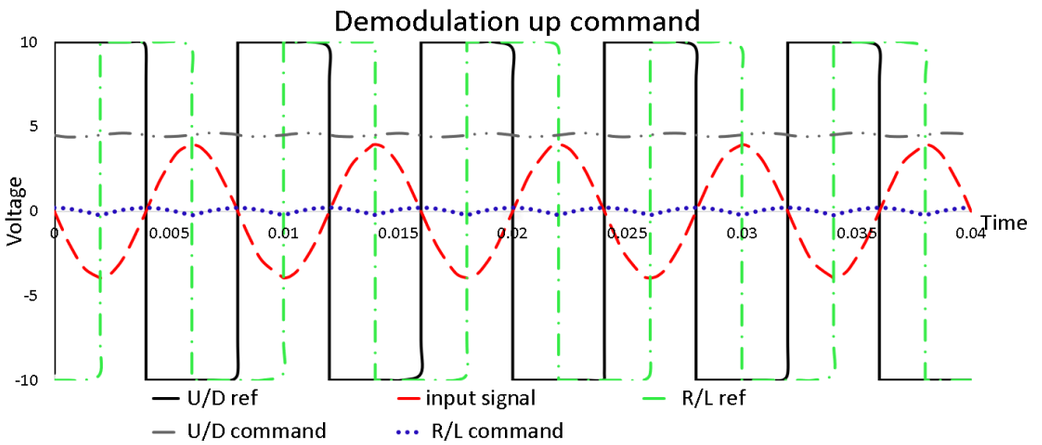

Fig. 7: Demodulation I/O simulated signals up-command

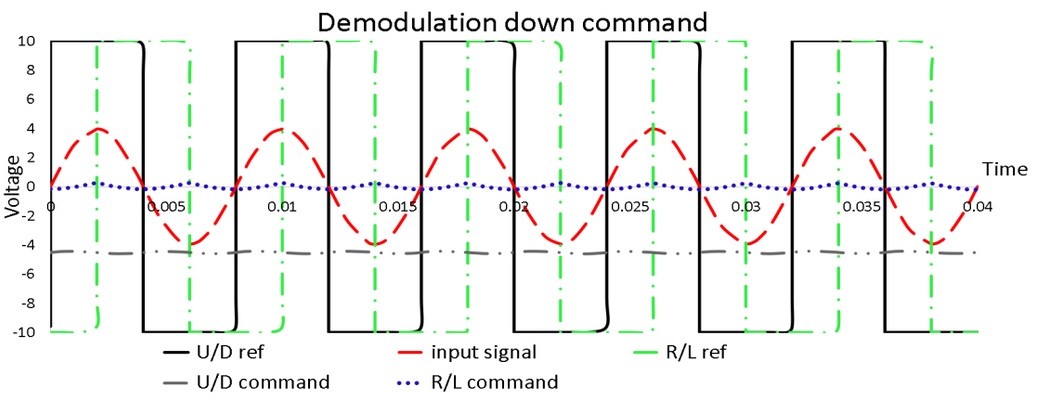

Fig. 8: Demodulation I/O simulated signals down-command

5- Design of Embedded System Servo Controller

The designed embedded system function description for both roll and yaw channels is shown in Figure (6). The microcontroller will be responsible for the servo system in a different phase where in boosting phase the velocity is too low for reliable aerodynamic control of the flight path. This could result in overcontrolling of the missile and unsuccessful flight. A slow enable function is added to the guidance path until effective control is established.

A microcontroller with 8-channels PWM Module, High-Speed 200 [ksps], 10-bits A/D Converter, External Clock modes up to 40 [MHz], 3 external interrupts, and 6 timers[11]. The software is developed with the MikroCTM environment. The ISR (interrupt service routine) is used to enable the guidance command exponentially for 2.75 [Sec]. Zero fin deflection achieved by 30% duty cycle for all solenoids with 6 [KHz].

The inputs for pitch feedback (pitch potentiometer) are

measured and subtracted from the pitch command after converting both of them into digital form. This subtracted value will be multiplied by a proportional controller gain K_p designed based on fine-tuning of the servo-identified model. The controller output is used to increase PWM duty value to the solenoid meanwhile decrease the PWM duty to the opposite Solenoid as represented in Figure (9) until the desired fin deflection is achieved. Due to the symmetry between the pitch and yaw plane, the same sequence applies to the yaw plane.

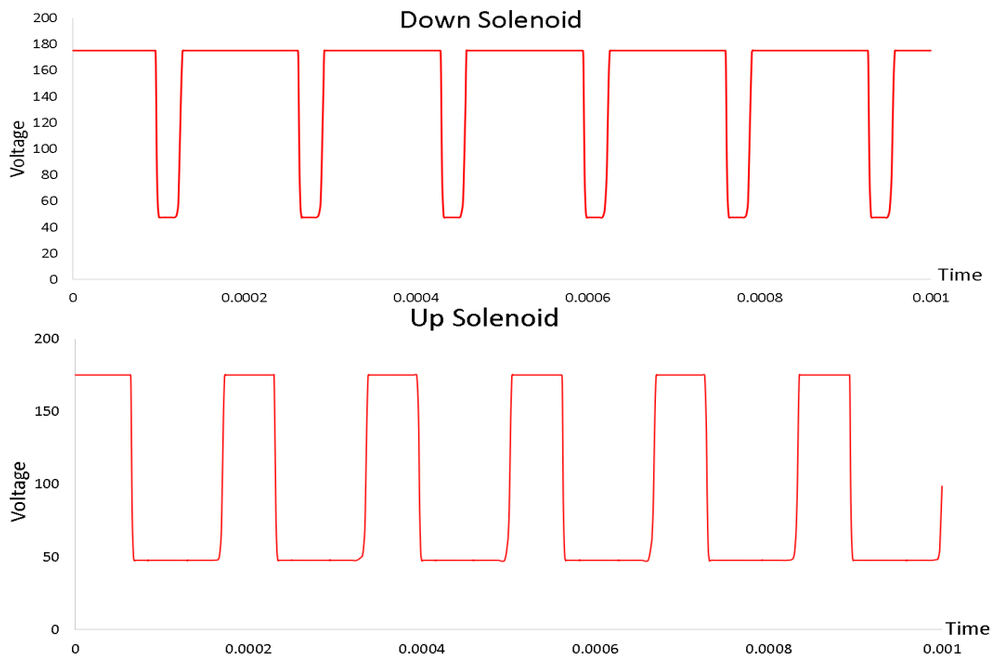

Fig. 9: Driving Circuit Output (PWM)

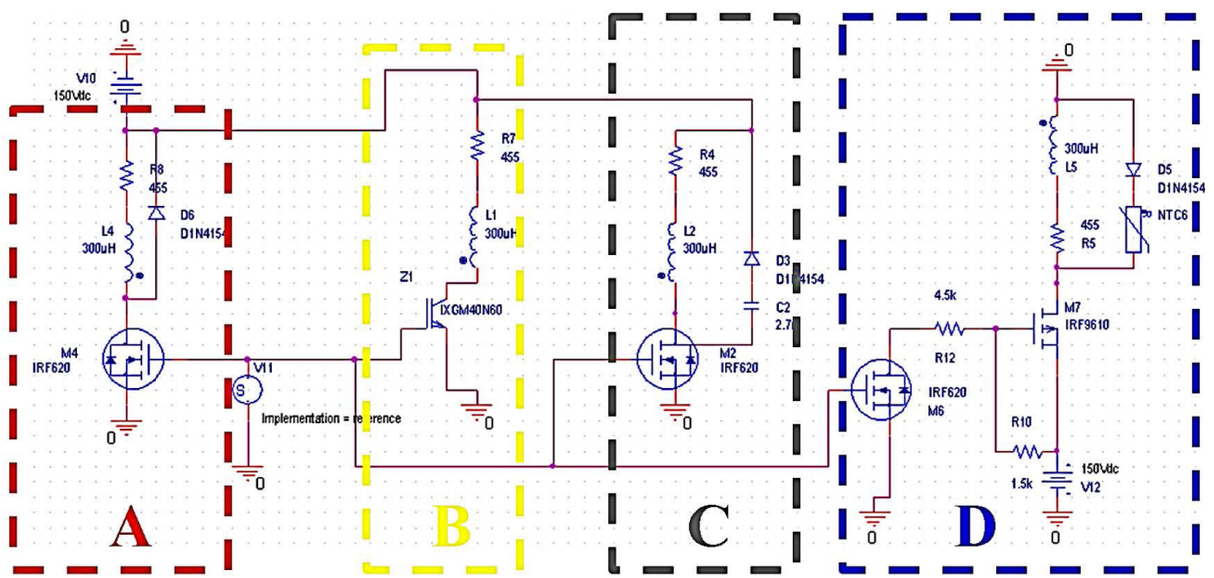

Fig. 10: Limiting Inductive Load Inrush Current Solutions

6-Design of Solenoid Driving Circuit (Actuator Driver)

It is the driving circuit that drives the solenoidsof the servo. Two different PWM duties with 5 [volt] amplitude are the inputs for both pitch and yaw channels and the output for each channel is the same input PWM voltage with 150 [Volt] D.C amplitude and 6 [KHz] frequency delivered by power MOSFETs used to drive a pair of solenoids in each plane. MOSFETs are increasingly used in driving high-power circuits and components it's preferred due to their high current handling capability. In this section there are three approaches will be represented according to the evaluation through OrCADTM simulation and the best performance selected for the solenoid valve for the pneumatic servo system driving. The solenoid valve is an inductive load so high inrush current needs attention must be given to the load characteristics where MOSFETs could be damaged if their voltage rating is exceeded because the spikes generated from inductive loads may have tremendous energy content and usually, some means of limiting their amplitude must be provided.In addition, the transient power generated during the turn-on and turn-off intervals must be determined in order to check for excessive channel temperatures. Highly inductive loads may generate significant power on turn-off,usually, with inductive loads, the peak voltage spike should be limited to a value below the breakdown rating of the transistor. Three techniques are commonly employed free-wheeling diodes and snubbing. Typical circuits are shown in Figure (10) the different designs controlled with the same control signal simulation PWM and powered with the same value 175 [Volt] D.C. And the typical equivalent value for the solenoid impedance Z (R=455 [Ω] and L= 300 [μH]). In design B the MOSFET was used without any voltage peak limitation showing that Figure (11) driving voltage peak overshooting to more than 300 [Volt] which is cause MOSFET failure.

Free-wheeling diodethe spikes caused by most electromechanical inductive loads such as solenoids or relays are effectively handled by the free-wheeling diode in model A in Figure (10). The low impedance of the diode usually causes the current to have a long decay time, however, which may be intolerable in some applications. Speed may be traded for overshoot voltage, by using resistance in series with the diodeHowever, junction rectifiers do exhibit a turn-ON transient which may allow excessive overshoot if the MOSFET is being driven off rapidly. In our case, a free-wheeling diode causes delayed voltage drop-out when power is removed, because current continuesto circulate in the diode and solenoid. As shown in Figure (11) the voltage didn't back to zero when the MOSFET is open.

The R-C snubberis commonly used in power conversion circuits to limit spikes caused by transformer leakage inductance and wiring inductance. It also reduces power dissipation by shaping the load line to appear more resistive. Resistor R, in series with the capacitor, is required to limit the inrush current turn-ON and to ensure that the circuit is adequately damped. Since the circuit is a resonant tank, it will exhibit a damped oscillation unless the circuit Q is 0.5 or less that are usually empirically determined. The peak voltage across the network will not exceed that calculated using the energy relationship $LI^2=CV^2$ Solving for the voltage, it is found that$V=I\sqrt{(L/C)}$.

The resonant frequency can be calculated from the usual relationship and R is selected so that $Q \backsim 1/2$ by using the relation $R=4\pi fL$. The equations and experience indicate that larger values of C lower the peak voltage and resonant frequency and consequently the resistor also must be reduced. An optimum value exists for a given L-C combination which resultsin minimum overshoot[12]. Finally, as shown in Figure (11) model C it's better than the free-wheeling diode but it still overshooting with more than 15 [Volt] D.C when the transistor is ON.

Current limiting thermistor NTCmodel D design two power MOSFETs used. IRL620 N-channel MOSFET in the low side which is driven by logic level so we could drive the gate to a source with an output of 5 [Volt] microcontroller and turn this MOSFET OFF fully[9]. The second one is IRFP9240 P-channel[13] Power MOSFETs is the simplified gate driving technique in high-side works up to -200V, continuous drain current up to -12 [Amp] at 10 [Volt] finally it could afford 150 [Watt] power dissipations but it's not logic level so we have to drive the gate to the source with -10 volts to drive it fully. Therefore, the low-side MOSFET is used to drive it. when the microcontroller 5 [Volt] is applied to the low side MOSFET gate it turns ON the drain will be connected to the ground generating a potential difference between gate and source which are connected through a resistor and by grounding the gate it will be more negative than the source so the high side P-Channel MOSFET will be ON and working with the diode as a switch to alternately applied voltage and ground to the solenoid and there is thermistor NTC add to limit the inrush current at turn-ON by their relatively high cold resistance as shown in Figure (12) As soon as, the inductive load is drawn current the thermistor temperature increase and its resistance decrease by a factor of 10 to 50 so it's able to handle inrush current effectively better than the fixed resistors without consuming too much power Finally, as represented in Figure (11). model D show it's the best performance despite 1.5 [μSec] fulling time, it does not affect the mechanical actuator like a pneumatic servo.

7- Proposed Design Simulation Result and testing verification

The proposed design has been tested and evaluated by using ATE(Automatic Test Equipment). The fin alignment test station evaluates the functionality and performance. Through many tests, nodes ensure integration with the other circuit cards. this test is represented in six tests nodes numerically displayed that show the performance enhancement as follows:

- Fin alignment for Right-Left plane.
- Fin alignment for Up-Down plane.
- Closed Loop Gain Right command.
- Closed Loop Gain Left command.
- Closed Loop Gain Up command.
- Closed Loop Gain Down command.

The ATE in Figure (13) uses the average value of four LVDTs (Linear Variable Differential Transformer) to measure the fin deflection from the null value at the minimum

guidance command signal. The minimum guidance command signal is achieved by moving

the target (mirror) in two planes and the black body temperature in the IR source is adjusted by the IR source controller to simulate the target signature. The test results are normalized and tabulated in Table 1, Table 2

The bar chart shown inFigure (14) demonstrates the results with the embedded-based circuit that is better in the fin alignment in the R/L plane, and U/D plane the enhancement percentage in each test. This enhancement is achieved because of replacing the fin adjustment potentiometer in the analog circuit which is adjusted manually based on the operator sensitivity with Digital fin Adjustment by generating the same PWM for every two opposite solenoids and fine adjustment is carried out with the aid of feedback.

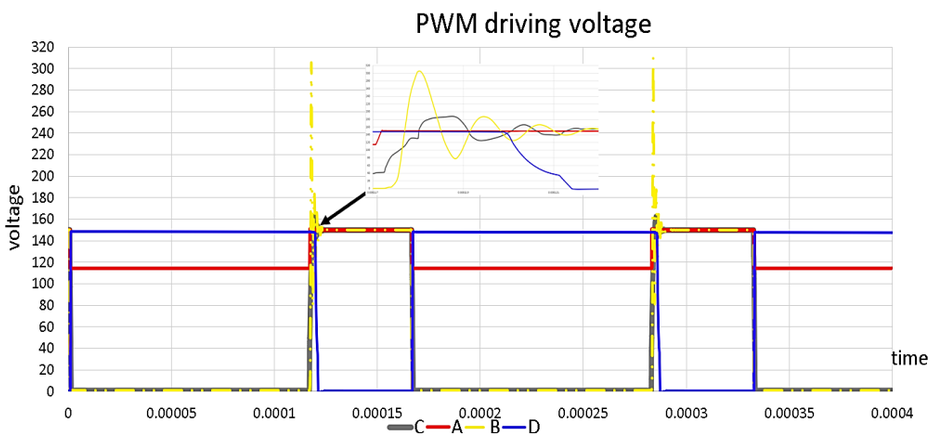

Fig. 11: Inductive load drivers' response

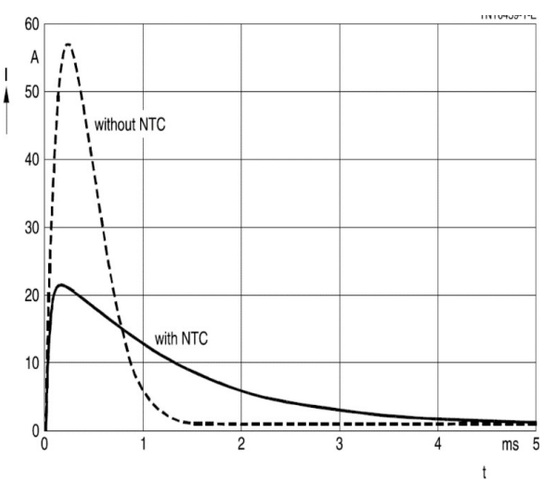

Fig. 12: Inrush current curves in a D.C circuit

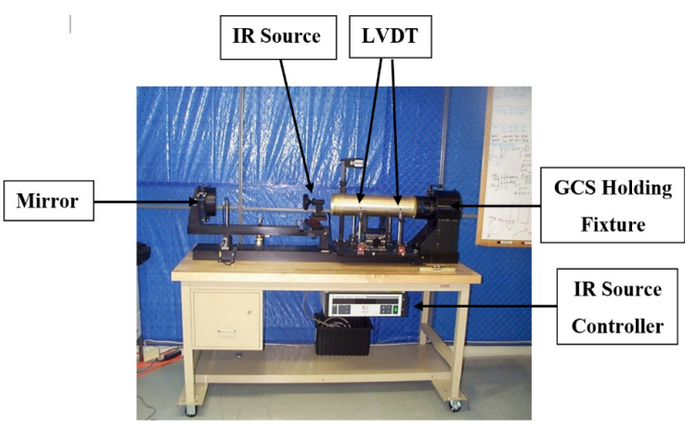

Fig. 13: ATE for testing snd validation

Table 1: Experimental Fin Alignment Results

Test Name	Deviation in Embedded circuit	Deviation in Analogue circuit	Enhancement percentage
Fin alignment for R/L plane	0.039126	0.194416	62.7%
Fin alignment for U/D plane	0.065214	-0.1418616	30.6%

Table 2: Experimental Servo control System Results

Test Name	Deviation in embedded circuit	Deviation in Analogue circuit	Enhancement percentage
Closed Loop Gain Right command	-0.0224156	-0.49266	47.02%
Closed Loop Gain Left command	-0.0035411	-0.61982	61.62 %
Closed Loop Gain Up command	0.0655598	0.716561	65.1%
Closed Loop Gain Down command	-0.0521572	-0.45355	40.1%

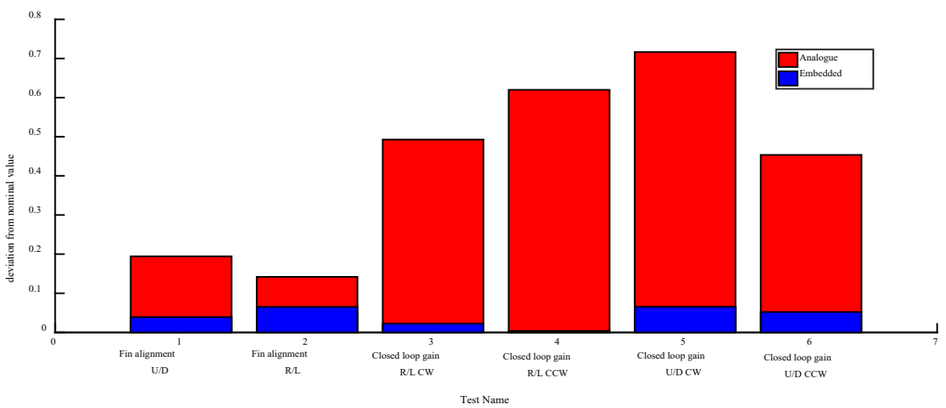

Fig. 14: ATE test results

8- Conclusion

This paper was devoted to obtaininga servo system model to improve the servo response through embedded circuit design. The black box pneumatic servo system identification is carried out using MATLABenvironment to be used in embedded controller design. The estimated model controller design is simulated for the selection of a suitable controller.

An embedded servo system controller based on a microcontroller is designed. Consequently, the pneumatic servo estimated using different models' electronic drivers for inductive load is demonstrated.

The proposed circuit based on the microcontroller was tested and evaluated using a standard ATE. Simulation and experimental results for the designed servo control system are given to illustrate the effectiveness of the presented technique.

References

[1] F. Ning, Y. Shi, M. Cai, Y. Wang, and W. Xu, "Research Progress of Related Technologies of Electric-Pneumatic Pressure Proportional Valves," Applied Sciences, vol. 7, no. 10, 2017, doi: 10.3390/app7101074.
[2] D. Saravanakumar, B. Mohan, and T. Muthuramalingam, "A review on recent research trends in servo pneumatic positioning systems," Precis Eng, vol. 49, pp. 481–492, 2017.
[3] A. Hildebrandt, R. Neumann, and O. Sawodny, "Optimal system design of siso-servopneumatic positioning drives," IEEE transactions on control systems technology, vol. 18, no. 1, pp. 35–44, 2009.
[4] B. P. Lathi, "Modern Digital and Analog Communication Systems (Oxford Series in Electrical and Computer Engineering)." Oxford University Press, 1998.
[5] J. C. Doyle, B. A. Francis, and A. R. Tannenbaum, Feedback control theory. Courier Corporation, 2013.
[6] O. Kaneko, S. Soma, and T. Fujii, "A FICTITIOUS REFERENCE ITERATIVE TUNING (FRIT) IN THE TWO-DEGREE OF FREEDOM CONTROL SCHEME AND ITS APPLICATION TO CLOSED LOOP SYSTEM IDENTIFICATION," IFAC Proceedings Volumes, vol. 38, no. 1, pp. 626–631, 2005, doi: 10.3182/20050703-6-CZ-1902.00105.
[7] R. L. Kosut, "System Identification for Robust Control Design.," 1996.

[8] S. F. Shelan, M. A. Hassan, H. Hendy, and Y. Z. Elhalwagy, "FPGA-based Controller For Electro-Mechanical Fin Actuation System Using Processor In The Loop (PIL)," in 2020 12th International Conference on Electrical Engineering (ICEENG), 2020, pp. 363–370. doi: 10.1109/ICEENG45378.2020.9171710.
[9] I. Gustavsson, L. Ljung, and T. Söderström, "Identification of processes in closed loop—identifiability and accuracy aspects," Automatica, vol. 13, no. 1, pp. 59–75, 1977.
[10] E. A. Lee and S. A. Seshia, Introduction to embedded systems: A cyber-physical systems approach. Mit Press, 2016.
[11] P. Yedamale, "Brushless DC Motor Control Using PIC18FXX31 MCUs," AN899 (Microchip Technology Inc.), 2004.
[12] L. Dos, L. Barbosa, B. Angélico, and C. Treviso, "A New Interleaved Boost PWM Soft Switched Converter," Dec. 2000.
[13] J. Abad Chico and others, "Realización de un amplificador de audio con etapa de salida a transistores MOSFET," 2019.